A. Frezzotti, H. Si Hadj Mohand, C. Barrot, S. Colin
Role of Diffusion on Molecular Tagging Velocimetry Technique for Rarefied Gas Flow Analysis
Microfluidics and Nanofluidics, Vol. 19, N. 6, 2015, p. 1335-1348
doi:10.1007/s10404-015-1649-2

Microfluidics Nanofluidics manuscript No.
(will be inserted by the editor)

Role of diffusion on molecular tagging velocimetry technique for rarefied gas flow analysis

Aldo Frezzotti · Hacene Si Hadj Mohand · Christine Barrot · Stéphane Colin

Received: date / Accepted: date

Abstract The Molecular Tagging Velocimetry (MTV) is a well-suited technique for velocity field measurement in gas flows. Typically, a line is tagged by a laser beam within the gas flow seeded with light emitting acetone molecules. Positions of the luminescent molecules are then observed at successive times and the velocity field is deduced from the analysis of the tagged line displacement and deformation. However, the displacement evolution is expected to be affected by molecular diffusion, when the gas is rarefied. Therefore, there is no direct and simple relationship between the velocity field and the measured displacement of the initial tagged line. This paper addresses the study of tracer molecules diffusion through a background gas flowing in a channel delimited by planar walls. Tracer and background species are supposed to be governed by a system of coupled Boltzmann equations, numerically solved by the Direct Simulation Monte Carlo (DSMC) method. Simulations confirm that the diffusion of tracer species becomes significant as the degree of rarefaction of the gas flow increases. It is shown that a simple advection-diffusion equation provides an accurate description of tracer molecules behavior, in spite of the non-equilibrium state of the background gas. A simple reconstruction algorithm based on the advection-diffusion equation has been developed to obtain the velocity profile from the displacement field. This reconstruction algorithm has been numerically tested on DSMC generated data. Results help estimating an upper bound on the flow rarefaction degree, above which MTV measurements might become problematic.

Keywords Molecular Tagging Velocimetry · Microflows · Direct Simulation Monte Carlo

PACS 47.45.Ab · 47.45.Gx · 47.61.Fg · 47.80.Cb

Aldo Frezzotti
Politecnico di Milano - Dipartimento di Scienze e Tecnologie Aerospaziali - Milano -Italy
Tel.: +39-02-23998358
Fax: +39-02-23998334
E-mail: aldo.frezzotti@polimi.it

Hacene Si Hadj Mohand · Christine Barrot · Stéphane Colin
Université de Toulouse, Institut Clément Ader, Toulouse, France

Mathematics Subject Classification (2000) 47N55

1 Introduction

Following the rapid development of microelectromechanical systems (MEMS) in the last decades, a number of new microfluidic applications involving gas microflows has emerged in various fields. For example, gas microflows are encountered in micro heat exchangers (Yang et al. 2014) designed for cooling electronic components or for chemical applications, in fluidic micro-actuators for active flow control (Cattafesta and Sheplak 2011), in micronozzles used for the micropropulsion of nanosats or picosats (Louisos and Hitt 2005), in micro gas chromatographs (μGCs) (Lu et al. 2005), in vacuum generators or Knudsen micropumps (Seungdo et al. 2014) as well as in some microfluidic-based in vitro devices (μFIVDs) such as artificial lungs (Kovach et al. 2015). Similar flows are also observed in porous media with applications relative to the extraction of shale gas (Niu et al. 2014).

In most of these systems, the Knudsen number Kn, ratio of the molecules mean free path over a characteristic length of the microsystem, is in the range $[10^{-3}, 10^{-1}]$ and the resulting slightly rarefied regime is the so-called slip flow regime, which is characterized by a velocity slip and a temperature jump at the wall (Colin 2005). Various theoretical models of these boundary conditions have been proposed in the literature and they involve accommodation coefficients which depend on the nature of the gas and the wall (Sharipov 2011); these models lead to more or less complex solutions for heat transfer (Colin 2012) and fluid flow (Zhang et al. 2012) in the slip-flow regime. Experimental data are then necessary to improve the critical discussion about the accuracy and limits of applicability of these slip boundary models. Experimental techniques described in the literature, however, mainly concern the measurement of global data (Morini et al. 2011). Most of the publications provide flowrate data through microchannels as a function of the pressure drop and the Knudsen number (Perrier et al. 2011; Ewart et al. 2006; Pitakarnnop et al. 2010; Maurer et al. 2003; Colin et al. 2004; Arkilic et al. 2001). This global information is not sufficient to separately analyze the role of the velocity slip model and the role of the a priori unknown accommodation coefficients. Unfortunately, there are few available data on local fields and most of them are pressure field data obtained by pressure-sensitive molecular films (PSMF) (Matsuda et al. 2011b,a). Up to now, there are no experimental data in the literature on velocity fields in rarefied gas microflows. For these reasons, it is crucial to develop accurate experimental velocimetry techniques adapted to the features of gas microflows.

For this goal, micro Molecular Tagging Velocimetry (μMTV) could be a well-suited technique able to avoid some difficulties associated to the more classic micro Particle Image Velocimetry (μPIV) technique, widely used for liquid microflows. The main limitation of μPIV for analyzing gas flows at microscale is linked to the Brownian motion of the small tracer particles, which makes difficult the cross-correlation process required to recognize particle patterns and extract velocity fields. For this reason, μPIV experiments in gases have been up to now limited to a few studies in millimetric channels and in non-rarefied regimes (Yoon et al. 2006; Sugii and

Okamoto 2006). On the other hand, the MTV technique is not based on a particle pattern identification. It relies on the properties of tracer molecules which can experience relatively long lifetime luminescence once excited with a light at an appropriate wavelength.

Typically, a laser beam is used to tag these molecules along a line (Lempert et al. 1995) or on a grid (Ismailov et al. 2006). Molecules luminescence is then detected at two successive times. The analysis of the tagged line or grid displacement and deformation allows the determination of the velocity field. As this little-intrusive technique uses molecular tracers, instead of particles, it presents several advantages compared with PIV. For example, in addition to the above-mentioned advantage, the repartition of the tracer is homogeneous and the risk of adhesion at the walls is limited. Nevertheless, at microscale, μMTV also presents some technological obstacles. First, its spatial resolution is constrained by the laser beam diameter, with a typical minimum value of the order of 30 μm, which requires operating in channels with a hydraulic diameter around 1 mm. For this reason, microflows in the slip flow regime should be analyzed with Knudsen similitude, reducing the pressure in order to reach Knudsen numbers in the range $[10^{-3}, 10^{-1}]$, corresponding to this regime. Second, although the Brownian motion is not an issue in itself, because the technique is not based on the recognition of a particle pattern, the diffusion of the molecular tracer within the main fluid could bias the measurement, and this effect can be increased with the reduction of pressure required to reach rarefied regimes. The efficiency of MTV has been demonstrated for liquid flows (Koochesfahani and Nocera 2007) at mini (Gendrich et al. 1997; Hu and Koochesfahani 2006) and micro (Thompson et al. 2005; Elsnab et al. 2010) scales. Its application to gaseous flows has been evidenced at millimetric scales in external flow configurations (Koochesfahani 1999; Stier and Koochesfahani 1999; Lempert et al. 2003; Pitz et al. 2005; ElBaz and Pitz 2012).

The first attempts to measure by MTV gas flows velocities inside devices with millimetric dimensions are recent (Samouda et al. 2012a,b). These preliminary measurements have been made in rectangular channels using one dimensional molecular tagging velocimetry (1D MTV); in this case a single line or a series of parallel lines are tagged perpendicularly to the flow direction. The component of the displacement is then obtained in the direction of the flow. Although 1D MTV has some limitations compared with 2D MTV and stereoscopic (3D) MTV, its advantages are a simpler implementation and a higher spatial resolution in the vicinity of the wall (Hammer et al. 2013). This makes 1D MTV a very promising technique for capturing velocity slip at the wall observed in rarefied regimes.

However, even at atmospheric pressure, data processing of preliminary velocity profiles has shown several issues (Samouda et al. 2015). The tagged molecules are subject to significant molecular diffusion and the diffusion effects should be taken into account during the data processing. A typical image of μMTV in gas flow is shown in Figure 1. It concerns a flow of argon, seeded with acetone molecules, in near-atmospheric pressure and temperature conditions. The flow is going from left to right in a 1 mm depth and 5 mm width rectangular channel. The image is obtained in the developed flow region, in the vertical plane of symmetry of the channel. The laser beam has tagged a line which emits fluorescence a few ns after tagging. The diameter

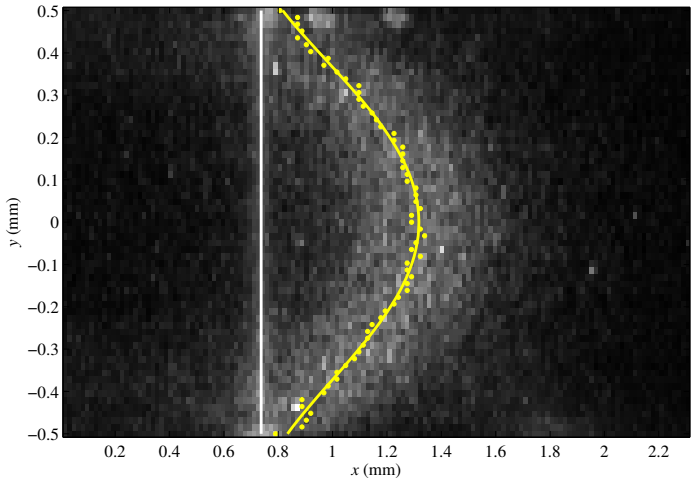

Fig. 1 Initial and deformed tagged lines in the developed flow or argon seeded by acetone molecules in the symmetry plane of a 1 mm height rectangular microchannel. $P_{in} = 105.7$ kPa, $P_{out} = 103.7$ kPa, $T_0 = 294$ K and $\Delta t = 100$ μs. Vertical white straight line: linear fit of the initial tagged line at $t = 0$; Yellow dots: tagged molecules displacements detected from maximum intensity of the signal at $t = 100$ μs, along each horizontal streamline; Curved yellow line: polynomial fit of tagged molecules displacements.

of the laser beam is 35 μm, and the fluorescence signal is easily and precisely fitted by the vertical green straight line. Phosphorescence is emitted 100 μs later and another image is obtained (both images are represented here in the same figure), revealing the gas displacement. The significant effect of diffusion is evidenced by the spreading of the phosphorescence signal. The maximum value of its intensity along each streamline determines the position of a yellow dot; finally the distribution of the yellow dots is fitted by a polynomial (the yellow curve in Figure 1). As explained in Section 4, the best fitting is found with a 4^{th} degree polynomial, although the expected velocity profile is parabolic. In addition, some slip is observed at both walls (the observed displacement is not zero), although in near-atmospheric conditions, the regime is still the continuum regime and no slip is expected at the wall. These two points demonstrate that the velocity profile cannot be directly deduced from the simple fit of the deformed tagged line observed after some delay following tagging. The effects of molecular diffusion have also been recently observed in liquid microflows by other authors who used photobleached molecular tracers for velocimetry purpose (Schembri et al. 2015). Although diffusion is much less significant in liquids, they showed that the velocity close to the walls could be overestimated due to the combination of molecular diffusion and shear.

In the present paper, a DSMC investigation of tagged molecules diffusion is performed to assist data processing from μMTV experiments in gas flows. The influence of the degree of rarefaction and of the gas composition is examined. A velocity reconstruction algorithm, based on the advection-diffusion equation, is then developed to be used as a tool for the interpretation and correct treatment of experimental data.

2 Problem formulation

In order to match the experimental setup (Samouda et al. 2012a,b, 2015), we consider the steady slow flow of a binary gas mixture in a long channel with rectangular section. The gas mixture is supposed to contain two components: the background gas species and the tracer gas species. The channel length, height and width are L_x, L_y and L_z, respectively. The length L_x is assumed to be much greater than L_y and L_z. Moreover, the channel height L_y is set to be smaller than L_z, to obtain an almost one-dimensional flow geometry where the prevailing gradients are aligned to y-direction in the central channel region. The experimental mixture flow is produced by applying different pressure values, P_{in} and P_{out}, at the channel inlet and outlet, respectively. The normalized pressure difference $\Delta P = \frac{P_{in}-P_{out}}{P_{in}}$ is set equal to a small value, in order to obtain a low Mach number and almost isothermal flow, with negligible gradients across the channel length.

The necessity of studying the effects of tracer molecules diffusion on the reconstruction of background gas velocity field as a function of the degree of gas rarefaction, forces the adoption of a kinetic theory description for the considered flows. Accordingly, it is assumed that the mixture behavior is governed by the following system of two coupled Boltzmann equations (Ferziger and Kaper 1972):

$$\frac{\partial f_i}{\partial t} + \boldsymbol{v} \circ \frac{\partial f_i}{\partial \boldsymbol{r}} = \sum_{j=1}^{2} Q_{ij}(f_j, f_i), \quad i = 1,2. \tag{1}$$

In Eqs. (1), $f_i(\boldsymbol{r}, \boldsymbol{v}|t)$ denotes the distribution function of atomic velocities $\boldsymbol{v}$ of species i, at spatial location $\boldsymbol{r}$ and time t. Species indexes 1 and 2 are attributed to the background and tracer species, respectively. It should be noted that, although the background gas could be either monatomic or polyatomic, the tracer gas has to be composed by optically active molecules with internal rotational and vibrational degrees of freedom. However, the detailed internal molecular structure is not believed to play a role in the considered almost isothermal flows whose properties are determined by overall collision cross sections. Moreover, the negligible temperature variations allow modeling molecular interactions through simple hard sphere potentials. Therefore, it is assumed that species i is composed by identical spherical atoms of mass m_i and diameter σ_i. The values of atomic diameters can be determined from the mixture viscosity and diffusion coefficient (Ferziger and Kaper 1972). The collision integral (Ferziger and Kaper 1972) Q_{ij}, which describes the mechanical interaction between species i and j, has the following expression:

$$Q_{ij}(f_j, f_i) = \frac{{\sigma_{ij}}^2}{2} \int_{\mathscr{S}^2} d^2\hat{\boldsymbol{k}} \int_{\mathscr{R}^3} d\boldsymbol{w} \left[f_j(\boldsymbol{r}, \boldsymbol{w}^*|t) f_i(\boldsymbol{r}, \boldsymbol{v}^*|t) - f_j(\boldsymbol{r}, \boldsymbol{w}|t) f_i(\boldsymbol{r}, \boldsymbol{v}|t) \right] |\boldsymbol{v}_r \circ \hat{\boldsymbol{k}}|, \tag{2}$$

where $\sigma_{ij} = \frac{\sigma_i + \sigma_j}{2}$.

In Eq. (2), the vector $\hat{\boldsymbol{k}}$, belonging to the unit sphere $\mathscr{S}^2$, specifies the relative position of two atoms at the time of their impact with relative velocity $\boldsymbol{v}_r = \boldsymbol{w} - \boldsymbol{v}$. The velocities $\boldsymbol{v}^*$ and $\boldsymbol{w}^*$, which are turned into $\boldsymbol{v}$ and $\boldsymbol{w}$ in a restituting collision, are

defined as (Ferziger and Kaper 1972):

$$\boldsymbol{v}^* = \boldsymbol{v} + 2\frac{m_j}{m_i+m_j}(\boldsymbol{v}_r \circ \hat{\boldsymbol{k}})\hat{\boldsymbol{k}}, \tag{3}$$

$$\boldsymbol{w}^* = \boldsymbol{w} - 2\frac{m_i}{m_i+m_j}(\boldsymbol{v}_r \circ \hat{\boldsymbol{k}})\hat{\boldsymbol{k}}. \tag{4}$$

Macroscopic quantities associated with the mixture flow are obtained as moments of the distribution functions. Partial and total number and mass densities are respectively defined as:

$$n_i(\boldsymbol{r},t) = \int f_i(\boldsymbol{r},\boldsymbol{v}|t)\, d\,\boldsymbol{v}, \qquad n(\boldsymbol{r},t) = \sum_{i=1}^{2} n_i(\boldsymbol{r},t) \tag{5}$$

$$\rho_i(\boldsymbol{r},t) = m_i n_i(\boldsymbol{r},t), \;\; \rho(\boldsymbol{r},t) = \sum_{i=1}^{2} \rho_i(\boldsymbol{r},t). \tag{6}$$

The molar fraction, $\chi_i(\boldsymbol{r},t)$, of the $i-th$ component and its mass fraction or concentration, $\tilde{\chi}_i(\boldsymbol{r},t)$, are defined as:

$$\chi_i(\boldsymbol{r},t) = \frac{n_i(\boldsymbol{r},t)}{n(\boldsymbol{r},t)}, \quad \tilde{\chi}_i(\boldsymbol{r},t) = \frac{\rho_i(\boldsymbol{r},t)}{\rho(\boldsymbol{r},t)}. \tag{7}$$

The mean velocity of each component is obtained as:

$$\boldsymbol{u}_i(\boldsymbol{r},t) = \frac{1}{n_i(\boldsymbol{r},t)} \int \boldsymbol{v} f_i(\boldsymbol{r},\boldsymbol{v}|t)\, d\,\boldsymbol{v}. \tag{8}$$

The hydrodynamic velocity, associated with the overall local mixture momentum, is defined as:

$$\boldsymbol{u}^{hyd}(\boldsymbol{r},t) = \frac{\sum_{i=1}^{2} \rho_i(\boldsymbol{r},t)\boldsymbol{u}_i(\boldsymbol{r},t)}{\rho(\boldsymbol{r},t)}. \tag{9}$$

The diffusion velocities $\boldsymbol{V}_i = \boldsymbol{u}_i - \boldsymbol{u}^{hyd}$ characterize the different velocities of the mixture components with respect to the common hydrodynamic velocity $\boldsymbol{u}^{hyd}$. Single component temperature T_i and overall mixture temperature T can be associated with velocity dispersions with respect to the hydrodynamic velocity, as follows:

$$\frac{3}{2} n_i(\boldsymbol{r},t) k_B T_i(\boldsymbol{r},t) = \frac{1}{2} m_i \int (\boldsymbol{v} - \boldsymbol{u}^{hyd})^2 f_i(\boldsymbol{r},\boldsymbol{v}|t)\, d\,\boldsymbol{v}, \tag{10}$$

$$\frac{3}{2} n(\boldsymbol{r},t) k_B T(\boldsymbol{r},t) = \sum_{i=1}^{2} \frac{1}{2} m_i \int (\boldsymbol{v} - \boldsymbol{u}^{hyd})^2 f_i(\boldsymbol{r},\boldsymbol{v}|t)\, d\,\boldsymbol{v}. \tag{11}$$

The boundary condition, at a generic position $\boldsymbol{r}_w$ on channel walls, is assigned following Maxwell's gas-surface interaction model (Cercignani 1988), which allows specifying the surface temperature T_w and species accommodation coefficients α_i in the range $[0,1]$. Atoms of species i impinging on one of the channel walls with velocity $\boldsymbol{v}$ are scattered back into the gas with velocity $\boldsymbol{v}'$ which is the result of a specular

reflection with probability $1-\alpha_i$ or diffuse reemission with probability α_i. In the latter case, the distribution functions of re-emitted atoms is the Maxwellian f_{wi}, defined as:

$$f_{wi}(\boldsymbol{r}_w, \boldsymbol{v}|t) = \frac{n_{wi}(\boldsymbol{r}_w|t)}{(2\pi R_i T_w)^{3/2}} \exp\left(-\frac{\boldsymbol{v}^2}{2R_i T_w}\right), \quad \boldsymbol{v}\circ\boldsymbol{n} > 0. \tag{12}$$

The gas constants are defined as $R_i = k_B/m_i$, being k_B the Boltzmann constant. The unit vector $\boldsymbol{n}$ is the normal to wall surface, pointing toward the gas region. Each amplitude n_{wi} is determined by requiring that the reemitted flux equals the impinging flux $-J_i^-$.

$$n_{wi}\sqrt{\frac{R_i T_w}{2\pi}} = -J_i^-, \qquad J_i^- = \int_{\boldsymbol{v}\circ\boldsymbol{n}<0} (\boldsymbol{v}\circ\boldsymbol{n}) f_i(\boldsymbol{r}_w, \boldsymbol{v}|t)\, d\boldsymbol{v}. \tag{13}$$

In view of the applications described below, it is convenient to define the overall mean free path λ_0 and mean free time τ_0 in an equilibrium state of the mixture, characterized by temperature T_0 and component species number densities n_{0j}:

$$\lambda_0 = \sum_{i=1}^{2} \chi_{0i} \left(\frac{1}{\sum_{j=1}^{2} n_{0j}\pi\sigma_{ij}^2 \sqrt{\frac{m_i+m_j}{m_j}}} \right) \tag{14}$$

$$\tau_0 = \frac{\lambda_0}{\sqrt{\frac{k_B T_0}{m_0}}} \tag{15}$$

where $m_0 = \sum_{i=1}^{2} \chi_{0i} m_i$ is the average molecular mass.

3 DSMC simulations of tagged molecules diffusion

The system defined by Eqs. (1) is solved by Direct Simulation Monte Carlo (DSMC) method (Bird 1994). The method numerically solves the *unsteady* form of the underlying kinetic equation. Steady solutions are found as the long time limit of unsteady ones. In DSMC distribution functions are represented by thousands of simulated molecules, each of them representing a large number of real molecules. The microscopic variables of simulated molecules (positions, velocities, internal states) evolve in time through a sequence of time steps, each consisting of two sub-steps: free flight and local binary collisions. The first one corresponds to the streaming operator at the l.h.s of Eqs. (1). Accordingly, only particles positions are updated, unless a collision with walls occurs and the particle velocity is also changed, as dictated by the assumed gas-surface interaction model (Cercignani 1988). During the second sub-step, particles are sorted into the cells of a conveniently defined spatial grid, their positions are kept fixed whereas velocities are changed by collisions, following stochastic rules consistent with the structure of the collision terms given by Eq. (2). Local macroscopic flow properties are obtained by sampling and time averaging molecules microscopic variables in each cell. The role of DSMC simulations in the research activity described here is twofold. The first one is to provide numerical solutions of the system of Boltzmann equations, governing the motion of background

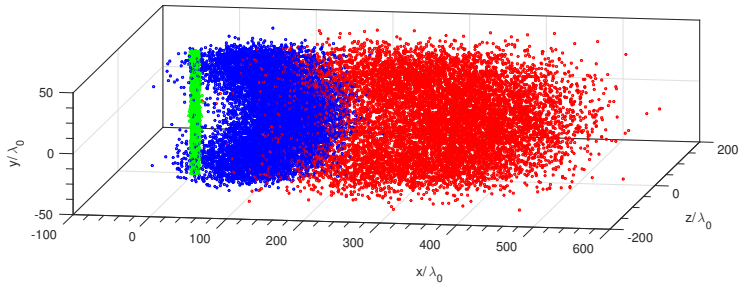

Fig. 2 Force driven Poiseuille flow of an Argon-Acetone mixture. $Kn = \frac{\lambda_0}{L_y} = 0.01$, $m_2/m_1 = 1.452$, $\sigma_2/\sigma_1 = 1.885$, $\chi_2 = 0.05$. Tagged molecules spatial distributions at times: $t_{tag} + 5.0\tau_0$ (green markers), $t_{tag} + 1000\tau_0$ (blue markers), $t_{tag} + 3000\tau_0$ (red markers).

and tracer gases, to study the influence of the gas rarefaction degree and gas-wall interaction, without assumptions beyond those intrinsic in the kinetic model itself. The second one is to provide well controlled simulations of tagged molecules diffusion in order to assess the accuracy of the velocity reconstruction method described below. It is worth observing that, in the present context, the inevitable statistical noise associated with DSMC simulations is a quite useful feature of the method because it allows investigating the robustness of the reconstruction against numerical data presenting noise levels made comparable to experimental ones.

A first example of the application of DSMC to the simulation of tracer species diffusion is given in Figures 2 and 3. The presented results have been obtained from spatially one-dimensional simulations of a binary hard spheres mixture Poiseuille flow between two infinite parallel plates. The geometry corresponds to the limit case in which both the channel width L_z and length L_x tend to infinity. The pressure gradient along the channel axis is replaced by a constant and uniform force field $\boldsymbol{F} = F_x\hat{\boldsymbol{x}}$ acting on both species. The balance of the volume force $\boldsymbol{F}$ and viscous stresses produces a steady flow of the mixture exhibiting the typical velocity profile, close to a parabolic shape. The intensity of the velocity maximum is controlled by F_x and it is set to a small fraction of the sound speed in order to obtain a slow isothermal flow. Full accommodation ($\alpha_1 = \alpha_2 = 1.0$) is assumed to occur at both walls having the same temperature T_w, set equal to the reference temperature T_0. The molar fraction of the tracer species χ_2 is set equal to 0.05, the mass ratio m_2/m_1 and the hard sphere diameter ratio σ_2/σ_1 are set respectively equal to 1.452 and 1.885 to mimic the argon-acetone mixture used in the experiments. In particular, hard sphere diameters have been obtained from the mixture components viscosities values at room temperature. Finally, the flow reference Knudsen number, $Kn = \lambda_0/L_y$, based on the channel height L_y and the reference mixture mean free path λ_0 is equal to 0.01. Tracer molecules diffusion is studied by the analysis of the relative positions

$$\boldsymbol{\delta}_i(t) = [x_i(t) - x_i(t_{tag})]\hat{\boldsymbol{x}} + y_i(t)\hat{\boldsymbol{y}} + [z_i(t) - z_i(t_{tag})]\hat{\boldsymbol{z}} \quad i = 1, \ldots, N_T \tag{16}$$

of N_T simulated tracer species particles, with respect to the reference initial position they have at a specified simulation time t_{tag}.

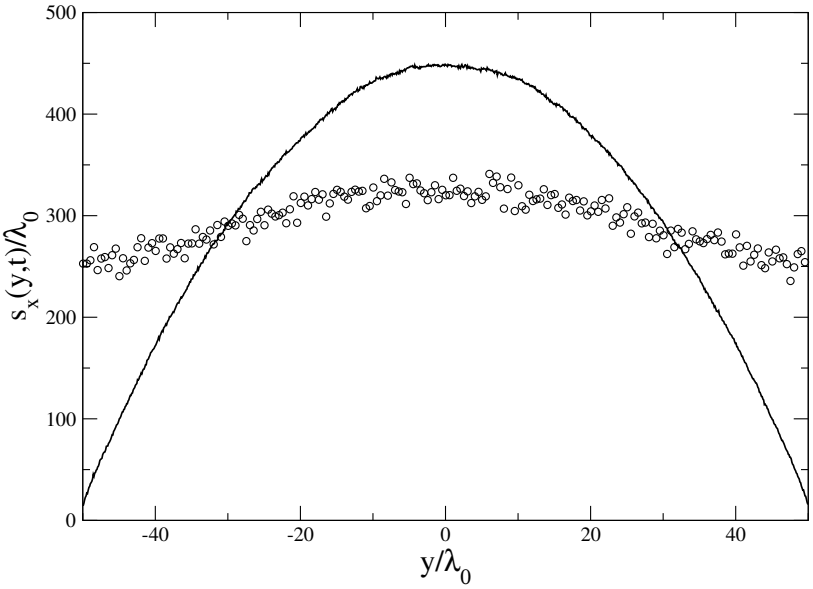

Fig. 3 DSMC computed tagged molecules average displacement $s_x(y,t)$ (circles) is compared with the nominal displacement $u_x(y)(t-t_{tag})$ (solid line) at time $t = t_{tag} + 3000\tau_0$. Flow setup as in Figure 2

Fixing reference molecular positions at $t = t_{tag}$ is the numerical analogue of the experimental laser shot used for molecular tagging. The time t_{tag} can be freely specified within the total simulation time, provided it is large enough to allow for the onset of steady flow conditions.

As Eq. (16) shows, at time t_{tag} particles relative positions occupy a straight line across the channel height, corresponding to the initial laser tagged region. Green markers in Figure 2 represent the spatial distribution of tracer species at a time very close to t_{tag}, when the ideal initial line has evolved into a thin cylinder, not yet significantly deformed by advection. The evolution of the initial line under the action of the stationary velocity field $\boldsymbol{u}^{hyd} = u_x(y)\hat{\boldsymbol{y}}$ and molecular diffusion is shown by the blue and red markers which represents the tagged molecules relative positions at times $t = t_{tag} + 1000\tau_0$ and $t = t_{tag} + 3000\tau_0$, respectively. The reference time, $\tau_0 = \lambda_0/\sqrt{R_1 T_w}$, is the mean free time in the reference equilibrium conditions mentioned above. It is evident that, although the flow Knudsen number is rather small, tagged particles displacements are considerably affected by diffusion which masks the pure particles advection caused by $\boldsymbol{u}^{hyd}$. A clearer assessment of the effects of diffusion on tagged particles displacements is provided by the analysis of the function $s_x(y,t)$ defined as:

$$s_x(y,t) = \frac{\int x n_2(x,y,z|t)\,dx\,dz}{\int n_2(x,y,z|t)\,dx\,dz}. \tag{17}$$

In Eq. 17, $n_2(x,y,z|t)$ is the number density of tracer molecules, hence $s_x(y,t)$ is the average displacement from the initial tagging positions of molecules having coordinate y along channel height, at time t. As shown in Figure 3, $s_x(y,t)$ is quite

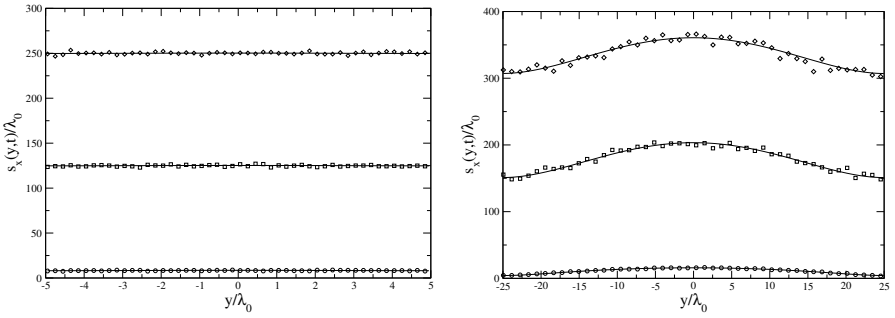

Fig. 4 Comparison of DSMC and diffusion equation predictions of tagged molecules average displacement $s_x(y,t)$ at $(t-t_{tag})/\tau_0 = 100, 1500, 3000$; solid lines: diffusion equation approximation (Eq. (49)); symbols: DSMC numerical solution of Eqs. (1). **Left** - *Argon-Acetone* mixture: $m_2/m_1 = 1.452$, $\sigma_2/\sigma_1 = 1.885$, $\chi_2 = 0.05$, $Kn = \lambda_0/L_y = 0.1$. **Right** - *Helium-Acetone* mixture: $m_2/m_1 = 14.49$, $\sigma_2/\sigma_1 = 3.136$, $\chi_2 = 0.05$, $Kn = \lambda_0/L_y = 0.02$

.

different from the nominal displacement $u_x(y)(t-t_{tag})$ that would occur if tracer molecules were simply transported along the channel with the background species velocity $u_x(y)$. Therefore, the reconstruction of the unknown velocity profile from the observed deformation of the initial tagged line requires that diffusion effects are subtracted from $s_x(y,t)$.

4 Diffusion equation approximation and velocity reconstruction

As described in Appendix A, the following evolution equation:

$$\frac{\partial s_x}{\partial t} = u_x(y) + \mathscr{D}_{12}\frac{\partial^2 s_x}{\partial y^2}. \tag{18}$$

can be derived for the average displacement $s_x(y,t)$, under the assumption that the simpler advection-diffusion Eq. (38) takes the place of the Boltzmann equations (1) to describe the motion of tracer species molecules. In Eq. (18), $u_x(y)$ is the steady, fully developed velocity field in the central region of the rectangular channel described above, whereas $\mathscr{D}_{12}$ is the diffusion coefficient of tracer molecules in the background gas. Eq. (18) can be solved in closed form, as described in Appendix A. An immediate consequence of Eq. (18) is that the area averaged displacement $\langle s_x\rangle(t) = \frac{1}{L_y}\int_{-\frac{L_y}{2}}^{+\frac{L_y}{2}} s_x(y,t)\,dy$ evolves in time as $\langle s_x\rangle(t) = \langle u_x\rangle t$, being $\langle u_x\rangle = \frac{1}{L_y}\int_{-\frac{L_y}{2}}^{+\frac{L_y}{2}} u_x(y)\,dy$ the time independent average flow rate per unit mass. Then, any solution $s_x(y,t)$ can be conveniently expressed in the form:

$$s_x(y,t) = \langle u_x\rangle t + s_\infty(y) + \tilde{s}_x(y,t). \tag{19}$$

The time independent contribution, $s_\infty(y)$, satisfies the equation

$$\frac{d^2 s_\infty}{dy^2} = \frac{1}{\mathscr{D}_{12}}\left[\langle u_x\rangle - u_x(y)\right] \tag{20}$$

being fully characterized by the conditions:

$$\left(\frac{d\,s_\infty}{d\,y}\right)_{y=\pm\frac{L_y}{2}}=0,\quad \frac{1}{L_y}\int_{-\frac{L_y}{2}}^{\frac{+L_y}{2}} s_\infty(y)\,dy=0. \tag{21}$$

The unsteady term, $\tilde{s}_x(y,t)$, obeys the one-dimensional homogeneous diffusion equation

$$\frac{\partial \tilde{s}_x}{\partial t}=\mathscr{D}_{12}\frac{\partial^2 \tilde{s}_x}{\partial y^2} \tag{22}$$

with initial and boundary conditions:

$$\tilde{s}_x(y,0)=-s_\infty(y),\quad \left(\frac{\partial \tilde{s}_x}{\partial y}\right)_{y=\pm\frac{L_y}{2}}=0. \tag{23}$$

Since $\tilde{s}_x$ decays exponentially in a time of the order of $L_y^2/\mathscr{D}_{12}$, the asymptotic behavior of $s_x(y,t)$ is a translation of the steady profile $s_\infty(y)$ with uniform velocity $\langle u_x\rangle$. The information about the velocity profile $u_x(y)$ carried by $s_x(y,t)$ is fully contained into the asymptotic part of the solution, whose structure can be illustrated by the following simple example. If it is assumed that the velocity profile has the parabolic shape

$$u_x(y)=a_0+a_2\frac{4}{L_y^2}\left(\frac{L_y^2}{4}-y^2\right) \tag{24}$$

which approximates the one-dimensional Poiseuille flow velocity profile when wall velocity slip is present, then it is immediately found that

$$\begin{aligned}\langle u_x\rangle &= a_0+\frac{2}{3}a_2\\ s_\infty(y) &= a_2\frac{L_y^2}{\mathscr{D}_{12}}\left[\frac{7}{720}-\frac{y^2}{3L_y^2}\left(\frac{1}{2}-\frac{y^2}{L_y^2}\right)\right].\end{aligned} \tag{25}$$

The "universal" factor between square brackets in Eq. (25) is a fourth degree polynomial whose variation across the channel height amounts to $1/48$. Therefore, the variation of $s_\infty(y)$ across the channel width, normalized to reference mean path λ_0, can be written as:

$$\Delta s'_\infty=\frac{[s_\infty(0)-s_\infty(+L_y/2)]}{\lambda_0}=\frac{a'_2}{48\mathscr{D}'_{12}Kn^2} \tag{26}$$

where $a'_2=a_2\sqrt{\frac{m_0}{k_BT_0}}$ and $\mathscr{D}'_{12}=\mathscr{D}_{12}\frac{\tau_0}{\lambda_0^2}$ are the normalized values of the velocity a_2 and diffusion coefficient, respectively. According to Eq. (26), the shape of $s_\infty(y)$ will be more evident at small rather than at high Knudsen numbers. Figure 4 presents two computational examples in which diffusion plays different roles. In the first one (see left panel), the Knudsen number is 0.1. In this case, the decay of $\tilde{s}(y,t)$ is extremely rapid and the depicted $s_x(y,t)$ profiles represent the asymptotic solution, consisting of the translation of a quite flat profile whose total variation is of the order of λ_0. In the second case, the Knudsen number is five times smaller and the normalized value

of $\mathscr{D}_{12}$ is also smaller because of the different mixture composition. Now the contribution of the transient term $\tilde{s}(y,t)$ is more evident, since the shape of profiles is changing, but it is no longer present in the two profiles at times $1500\tau_0$ and $3000\tau_0$, which exhibit a more pronounced curvature. In agreement with the above estimate, the variation of $s_\infty(y)$ is now close to $60\lambda_0$.
The results displayed in Figure 4 also show that it is possible to reproduce DSMC average displacement profiles by the advection-diffusion approximation with good accuracy, thus justifying the development of a simple method to reconstruct the unknown $u_x(y)$ from the observed $s_x(y,t)$, as described in the next section.

5 Velocity reconstruction

Although the unknown velocity profile could be reconstructed only on the basis of the asymptotic contribution to $s_x(y,t)$, it should be observed that the transient contribution $\tilde{s}_x(y,t)$ is also present at finite times, particularly when Kn is small. A simple method to obtain the velocity $u_x(y)$ from $s_x(y,t)$, which does not use the decomposition given by Eq. (19), can be formulated by writing $s_x(y,t)$ in the form:

$$s_x(y,t) = \int_{-L_y/2}^{L_y/2} G(y,y',t)u_x(y')\,dy'. \tag{27}$$

as shown in Appendix A.
Let $\{U_k(y), \quad k = 0,1,\ldots,N_u\}$ be a sequence of N_u *assigned* basis functions (typically polynomials), such that the gas velocity profile $u_x(y)$ can be approximated as:

$$u_x(y) = \sum_{k=0}^{N_u} a_k U_k(y). \tag{28}$$

The linearity of the direct relationship between $s_x(y,t)$ and $u_x(y)$, expressed by Eq. (27), immediately shows that

$$s_x(y,t) = \sum_{k=0}^{N_u} a_k S_k(y,t), \qquad S_k(y,t) = \int_{-L_y/2}^{L_y/2} G(y,y',t)U_k(y')\,dy'. \tag{29}$$

In words, the displacement can be written as a superposition of N_u *assigned* basis displacements $S_k(y,t)$. Each of them is obtained by solving Eq. (18) with the corresponding velocity $U_k(y)$, through Eq. (50).
The coefficients a_k of the superposition in Eq. (29) are the same appearing in the velocity expansion, defined by Eq. (28). Hence, the unknown velocity field can be determined by a least square approximation of $s_x(y,t)$, *i.e.* by minimizing the quadratic error $E_s = \left[s_x(y,t) - \sum_{k=0}^{N_u} a_k S_k(y,t)\right]^2$, where $s_x(y,t)$ is obtained from actual physical experiments or numerical simulations.

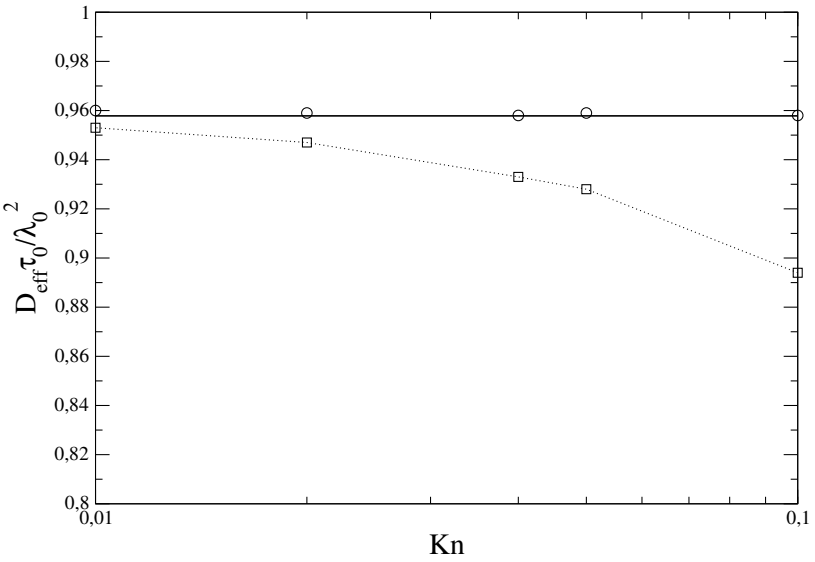

Fig. 5 Effective self-diffusion coefficient vs. Knudsen number in a pure hard sphere gas at rest between two parallel plates. □: $\alpha = 1$ (fully accommodating walls); ○: $\alpha = 0$ (specularly reflecting walls); solid line: normalized Chapman-Enskog value of $\mathscr{D}_{12}$ from Eq. (30)

.

6 Validation of the velocity reconstruction method

The capabilities of the velocity reconstruction method described in the previous section have been assessed by using DSMC simulations of tagged molecules diffusion in Poiseuille flows. As noted above, Eq. (49) provides a good approximation of DSMC average displacements $s_x(y,t)$, even when the reference Knudsen number is as high as 0.1 (see Figure 4). However, it should be observed that the accurate reproduction of DSMC simulations requires replacing the Chapman-Enskog value of diffusion coefficient $\mathscr{D}_{12}$ with an effective diffusion coefficient $\mathscr{D}_{eff}$ which takes into account the presence of walls when Kn grows (Dongari et al. 2009). For each mixture composition and reference Knudsen number, $\mathscr{D}_{eff}$ has been obtained from Einstein's formula $\langle x^2\rangle(t) = 2\mathscr{D}_{eff}t$ (Res 1977). The variance of molecular positions with respect to their initial values, $\langle x^2\rangle(t)$, has been computed by equilibrium DSMC simulations. Figure 5 shows how gas-surface interaction affects self-diffusion in a pure hard sphere gas confined between two infinite parallel plates, whose separation is L_y. When walls are fully accommodating ($\alpha = 1$), D_{eff} is a decreasing function of $Kn = \lambda_0/L_y$ which, for $Kn \to 0$, tends to the Chapman-Enskog value:

$$\mathscr{D}_{12} = \left(\frac{3\sqrt{\pi}}{2^{\frac{5}{2}}}\frac{\lambda_0^2}{\tau_0}\right) f_D. \tag{30}$$

In Eq. (30), the term in brackets is the first approximation to $\mathscr{D}_{12}$ which needs to be multiplied by f_D to obtain the fully converged value. Following the methods developed in (Bruno et al. 2006), the correcting factor f_D can be given the value 1.018954.

As expected, Kn independent estimates of D_{eff} are obtained for specularly reflecting walls. This case is equivalent to setting periodic boundary conditions at walls and to simulating diffusion in a virtually infinite and uniform background. Hence, the obtained D_{eff} coincides with the Chapman-Enskog value.
The possibility of reproducing DSMC results by the corresponding diffusion equation approximation justifies the attempt to reconstruct the unknown $\boldsymbol{u}^{hyd}$ from the observed $s_x(y,t)$ through the method described above. In order to evaluate the capabilities and the limitations of the velocity reconstruction method described in section 5, different sets of displacement data have been generated by DSMC simulations. Attention has been focused on the effects of rarefaction, by varying the reference Knudsen number in the range $[0.01, 0.1]$, and on the influence of the mixture mass ratio m_2/m_1. The latter parameter has been assigned the values $1.0, 1.452, 14.49$ to study respectively the limit case of equal mass for the tracer and background species, the argon-acetone and the helium-acetone mixtures. The influence of the statistical noise of the displacement data on the accuracy of the velocity reconstruction has been also analyzed by varying the number of DSMC particles used to simulate the tracer species. In all cases described below, the simplest velocity basis, consisting of the two elements

$$U_0(y) = 1, \quad U_2(y) = \frac{4}{L_y^2}\left(y^2 - \frac{L_y^2}{4}\right)$$

has been used for velocity reconstruction numerical experiments. Although representing the Poiseuille velocity profiles by a shifted parabola introduces a small systematic error at higher Kn values, the adopted choice is adequate for evaluating the reconstruction method and can be easily improved by adding additional basis functions.
For each DSMC simulation, N_s snapshots $s_x(y,t_k)$ of tracer species displacements have been taken at equally spaced times $\{t_k, k = 1,\ldots,N_s\}$, during a long period (typically $3000 - 4000\tau_0$) following the onset of steady flow conditions in the channel. The velocity reconstruction method has then been used on each $s_x(y,t_k)$ to obtain N_s estimates $u_x^{(k)}(y)$ of the reference velocity field $u_x(y)$, computed by the same DSMC simulation. A sequence of N_s reconstruction errors, normalized to the value of $u_x(y)$ at the channel center, has been computed as:

$$\varepsilon_v(t_k) = \frac{1}{u_x(0)}\frac{1}{L_y}\int_{-\frac{L_y}{2}}^{\frac{L_y}{2}} |u_x^{(k)}(y) - u_x(y)|\, dy. \tag{31}$$

Table 1 reports $\varepsilon_v(min)$, $\langle\varepsilon_v\rangle$ and $\varepsilon_v(max)$, respectively the computed minimum, average and maximum values of the sequence $\varepsilon_v(t_k)$, as functions of Kn, m_2/m_1 and displacement data noise level. The latter has been characterized by the quantities:

$$\varepsilon_d^2(t_k) = \frac{1}{L_y}\int_{-\frac{L_y}{2}}^{\frac{L_y}{2}} \left[s_x(y,t_k) - a_0 S_0(y,t_k) - a_2 S_2(y,t_k)\right]^2 dy \tag{32}$$

measuring the dispersion of the noisy DSMC $s_x(y,t_k)$ profiles with respect to their corresponding best fit, in terms of basis displacement functions. Since $s_x(y,t)$ is obtained as a mean value of a particle position population whose variance is a linearly

$m_2/m_1 = 1.0$

Kn	$\mathscr{D}_{eff}$	$N_T/Cell$	$a\ (\varepsilon_d = a\sqrt{t-t_{tag}})$	$\varepsilon_v(min)$, $\langle\varepsilon_v\rangle$, $\varepsilon_v(max)$
0.10	0.894	50	0.194	0.07, 1.7, 5.7
0.10	0.894	500	0.06	0.01, 0.52, 1.6
0.10	0.894	5000	0.019	0.01, 0.15, 0.47
0.05	0.928	50	0.198	0.02, 0.30, 1.40
0.05	0.928	500	0.06	0.006, 0.07, 0.2
0.04	0.933	50	0.198	0.06, 0.16, 0.46
0.04	0.933	500	0.06	0.007, 0.05, 0.14
0.02	0.947	50	0.20	0.006, 0.03, 0.10
0.02	0.947	500	0.06	0.006, 0.01, 0.03
0.01	0.953	50	0.21	0.004, 0.01, 0.02
0.01	0.953	500	0.07	0.006, 0.01, 0.02

$m_2/m_1 = 1.452, \quad Ar - C_3H_6O$

Kn	$\mathscr{D}_{eff}$	$N_T/Cell$	$a\ (\varepsilon_d = a\sqrt{t-t_{tag}})$	$\varepsilon_v(min)$, $\langle\varepsilon_v\rangle$, $\varepsilon_v(max)$
0.10	0.420	500	0.04	0.01, 0.19, 0.65
0.05	0.422	250	0.06	0.007, 0.04, 0.13
0.04	0.425	200	0.07	0.005, 0.03, 0.10
0.02	0.430	100	0.10	0.004, 0.01, 0.02
0.01	0.440	50	0.17	0.006, 0.008, 0.014

$m_2/m_1 = 14.49, \quad He - C_3H_6O$

Kn	$\mathscr{D}_{eff}$	$N_T/Cell$	$a\ (\varepsilon_d = a\sqrt{t-t_{tag}})$	$\varepsilon_v(min)$, $\langle\varepsilon_v\rangle$, $\varepsilon_v(max)$
0.10	0.142	500	0.025	0.01, 0.03, 0.10
0.05	0.144	250	0.04	0.006, 0.01, 0.03
0.04	0.145	200	0.05	0.004, 0.008, 0.014
0.02	0.146	100	0.09	0.003, 0.005, 0.008
0.01	0.147	50	0.13	0.005, 0.007, 0.01

Table 1 Velocity profile reconstruction error as a function of reference Knudsen number, for different noise levels of DSMC average displacement profile and mass ratios m_2/m_1. In all cases, tracer species molar fraction χ_2 is equal to 0.05.

increasing function of time, $\varepsilon_d(t)$ is well fitted by the function $\varepsilon_d(t) = a\sqrt{t-t_{tag}}$, as shown in the upper right panel of Figure 6. The amplitude a is roughly inversely proportional to the square root of number of samples used to estimate $s_x(y,t_k)$, as shown by the case $Kn = 0.1$, $m_2/m_1 = 1$ where increasing the number of tracer particles per grid cell from 50 to 5000 allows reducing the noise level by a factor 10. The importance of $\varepsilon_d(t)$ in determining ε_v strongly depends on the value of the Knudsen number. As discussed above, when Kn is of the order of 0.1, the transient contribution $\tilde{s_x}(y,t)$ decays rapidly and the displacement reduces to its asymptotic part, which exhibits an almost flat profile whose structure is easily hidden by the statistical noise. In this case, the reconstruction error is very high, unless $s_x(y,t)$ is determined with very high accuracy, as shown by the values reported in Table 1. In the light of the above considerations, it seems reasonable to assume that an accurate velocity field reconstruction from tagged molecules displacements requires that the normalized statistical error $\varepsilon_d(t)/\lambda_0$ associated with $s_x(y,t)$ is smaller than a quantity of the order of $\Delta s'_\infty$, the estimated size of the normalized variation of $s_x(y,t)$ across the channel, defined by Eq. (26).

An example of the unfavorable combination of relatively high values of Knudsen

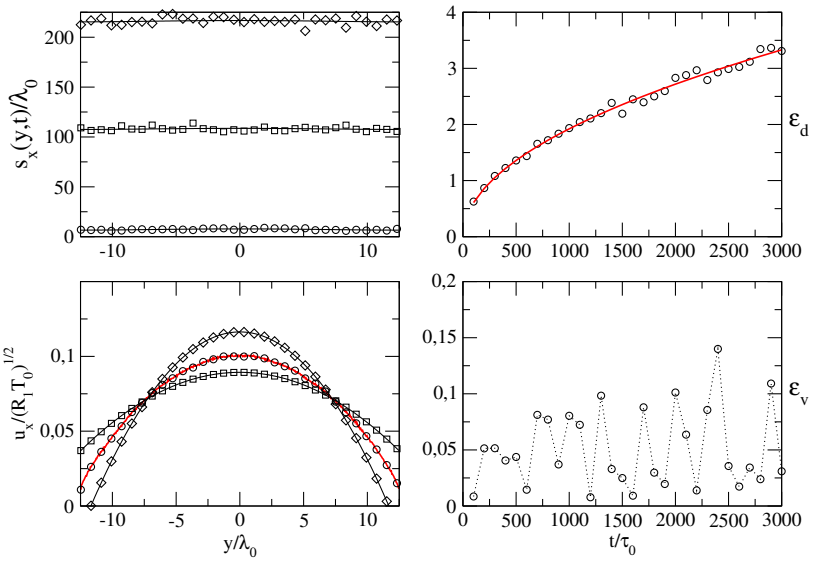

Fig. 6 $m_2/m_1 = 1.0$, $Kn = 0.04$. **Upper left**- $s_x(y,t)$ DSMC profiles at: $t = t_{tag} + 100\tau_0$ ($\circ$), $t = t_{tag} + 1500\tau_0$ ($\square$),$t = t_{tag} + 3000\tau_0$ ($\diamond$); solid lines represent best fits in terms of $S_0(y,t)$ and $S_2(y,t)$. **Upper right**- Time evolution of ε_d. $\circ$: DSMC data; solid line: best fit as $\varepsilon_d = a\sqrt{t - t_{tag}}$. **Lower left** - Velocity profiles reconstructed from displacements at $t = t_{tag} + 100\tau_0$ ($\circ$), $t = t_{tag} + 1500\tau_0$ ($\square$),$t = t_{tag} + 3000\tau_0$ ($\diamond$); red solid line: reference DSMC velocity profile in the channel. **Lower right** - Time evolution of velocity reconstruction error, ε_v.

number and diffusion coefficient is presented in Figure 6, showing the difficulty of extracting accurate estimates of $u_x(y)$ from quite flat displacement profiles, biased by statistical noise. For the same noise level, considerably lower values of ε_v are obtained at smaller Knudsen numbers, still in the slip flow regime. The $s_x(y,t_k)$ profiles are more pronounced, therefore reconstruction is less sensitive to noise, as shown in Figure 7, showing the time evolution of $s_x(y,t_k)$ and the comparison of reconstructed velocity profiles with the computed DSMC velocity in the case $m_2/m_1 = 1.452$ (Argon-Acetone mixture), $Kn = 0.02$. The comparison of ε_v data for the three mixtures also shows that, as is obvious, smaller values of the diffusion coefficient lead to better velocity profile reconstruction.
It is worth observing that, although the effective value, D_{eff}, of the diffusion coefficient has been used in velocity reconstruction numerical experiments, using its nominal value $\mathscr{D}_{12}$, resulting from Chapman-Enskog expansions, does not appreciably increase ε_v, since walls effect on diffusion are small, particularly for the mixtures considered here.

7 Conclusions

Tagged molecules diffusion in a background rarefied gas flowing through a channel has been studied by DSMC simulations, in order to support MTV measurements in microchannels. It has been shown that a simple diffusion equation describing the evo-

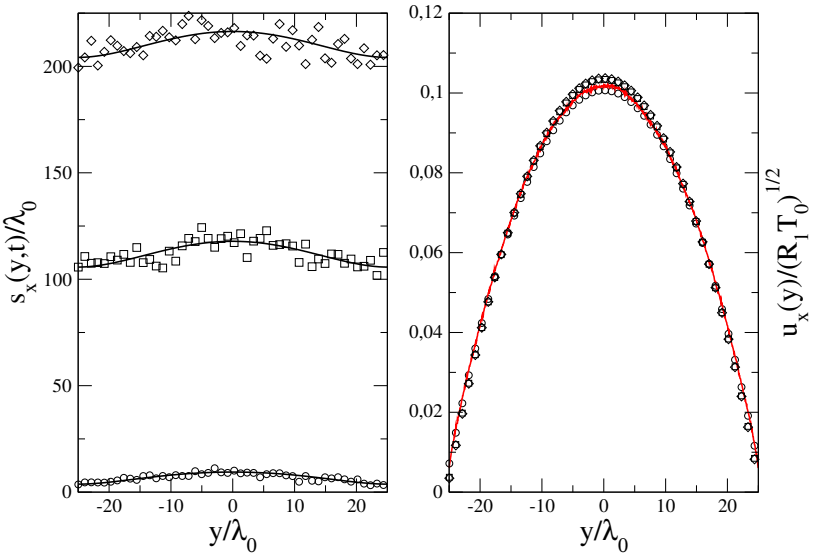

Fig. 7 $m_2/m_1 = 1.452$, $Ar - C_3H_6O$, $Kn = 0.02$, $\chi_2 = 0.05$. **Left**- $s_x(y,t)$ DSMC profiles at: $t = t_{tag} + 100\tau_0$ ($\circ$), $t = t_{tag} + 1500\tau_0$ ($\square$),$t = t_{tag} + 3000\tau_0$ ($\diamond$); solid lines represent best fits in terms of $S_0(y,t)$ and $S_2(y,t)$ functions. **Right** - Velocity profiles reconstructed from displacements at $t = t_{tag} + 100\tau_0$ ($\circ$), $t = t_{tag} + 1500\tau_0$ ($\square$),$t = t_{tag} + 3000\tau_0$ ($\diamond$); red solid line: reference DSMC velocity profile in the channel.

lution of the average displacement of tagged molecules provides a good description of DSMC numerical solutions of a system of coupled Boltzmann equation, if Knudsen number dependent diffusion coefficients are adopted to take into account wall effects. The diffusion equation approximation has also been used to formulate a simple method to reconstruct the velocity profile in the channel from the observed tagged molecules displacements. Using DSMC simulations as a source of data naturally affected by controllable statistical noise, it has been shown that velocity reconstruction becomes difficult at Knudsen numbers of the order of 0.1 but it becomes rapidly more accurate at lower values of Kn which still belong to the slip regime.
Although the kinetic theory formulation of the problem and the following advection-diffusion approximation have been based on a physical picture in which a negligible amount of tracers diffuse through a pure gas, the adopted methods do have wider validity. Actually, the more realistic case in which the tracer species is just one of the mixture components, present in any arbitrary amount, can be dealt with by an extended form of Eqs. (34,35), in which Eqs. (34) is replaced by two steady Boltzmann equations describing the stationary background flow. The unsteady equation (35) is replaced by the following linear equation:

$$\frac{\partial f_T}{\partial t} + \boldsymbol{v} \circ \frac{\partial f_T}{\partial \boldsymbol{r}} = Q_{21}(f_T, f_1) + Q_{22}(f_T, f_2) \tag{33}$$

in which f_T is the distribution of tracers. However, it is not necessary to think of tracers as a separate species, although mechanically identical to species 2, since Eq. (33) can be considered as a Lagrangian description of the motion of the same species 2, of

which the steady Boltzmann equations give the Eulerian view. The distinction is not even necessary in DSMC simulations in which any mixture component can also play the role of tracer species. As done above, it is then possible to assume that Eq. (33) can be replaced by the advection-diffusion equation (40) in which $\mathscr{D}_{12}$ is now the diffusion coefficient of a test tracer through the backgound mixture. The research work described here is intended as a first step which needs the application to real experimental data to take its final shape.

8 Acknowledgements

This research obtained financial support from the European Community's Seventh Framework Program (FP7/2007-2013) under grant agreement no 215504, from the Fédération de Recherche Fermat, FR 3089, and from the Project 30176ZE of the PHC GALILEE 2014 Program. The latter is supported by the Ministère des Affaires Etrangères et du Développement International (MAEDI) and the Ministère de l'Enseignement Supérieur et de la Recherche (MENESR).

A Diffusion approximation

Assuming that the tracer species is instantaneously added in negligible amount to the undisturbed steady flow of the background gas allows rewriting Eqs. (1) as follows:

$$\boldsymbol{v} \circ \frac{\partial f_1}{\partial \boldsymbol{r}} = Q_{11}(f_1, f_1) \tag{34}$$

$$\frac{\partial f_2}{\partial t} + \boldsymbol{v} \circ \frac{\partial f_2}{\partial \boldsymbol{r}} = Q_{21}(f_2, f_1). \tag{35}$$

The linear Eq. (35) describes the unsteady diffusion of tracer molecules through a non-equilibrium background by neglecting tracer molecules interaction ($Q_{22}(f_2, f_2) = 0$) and their effects on the background gas flow described by the non-linear Boltzmann equation (34).
As shown below, the kinetic equations, either in the general form expressed by Eqs. (1) or in the limit case described by Eqs. (34,35), can be effectively used to simulate tagged molecules diffusion. However, their mathematical form is too complicated to formulate a method for the reconstruction of the velocity field in the background gas from the observed displacement of tagged molecules.
A simpler description of tagged molecules transport is provided by the diffusion equation (Ferziger and Kaper 1972; Crank 1975):

$$\frac{\partial \rho_2}{\partial t} + \frac{\partial}{\partial \boldsymbol{r}} \circ (\rho_2 \boldsymbol{u}^{hyd}) = \frac{\partial}{\partial \boldsymbol{r}} \circ \left[\rho \frac{m_1 m_2}{(\rho/n)^2} \mathscr{D}_{12} \frac{\partial}{\partial \boldsymbol{r}} \left(\frac{\rho_2}{\rho} \right) \right] \tag{36}$$

where the binary diffusion coefficient $\mathscr{D}_{12}$ takes the following form:

$$\mathscr{D}_{12} = \frac{3}{16 n m_{12}} \frac{\sqrt{2\pi m_{12} k_B T}}{\pi \sigma_{12}^2}, \quad m_{12} = \frac{m_1 m_2}{m_1 + m_2} \tag{37}$$

in the first approximation of the diffusion coefficient of a binary mixture of hard sphere molecules. Eq. (36) can be derived from Eqs. (1) assuming that the scale of spatial gradients is much larger than the mean free path (Ferziger and Kaper 1972) and the contributions of pressure and temperature gradients to the diffusion driving force can been neglected. The contribution of the external force field $\boldsymbol{F}$ to the diffusion driving force is automatically cancelled, since both species are subject to the same force (Ferziger and Kaper 1972). In the considered geometry, $\boldsymbol{u}^{hyd}$ reduces to its axial component u_x which can be assumed to

depend only on y and z in the region accessible to tagged molecules during their luminescence life time. Hence, the velocity field divergence can be neglected and, for small χ_2 values Eq. (36) takes the form:

$$\frac{\partial n_2}{\partial t} + u_x(y,z)\frac{\partial n_2}{\partial x} = \mathscr{D}_{12}\nabla^2 n_2 - \frac{1}{\tau_p}n_2. \tag{38}$$

The diffusion coefficient $\mathscr{D}_{12}$ is assumed to be constant because of the small variation of temperature and density in the flowfield. The additional source term $-\frac{1}{\tau_p}n_2$ has been added at r. h. s. of the above equation to take into account the decay of tagged molecules number as a result of phosphorescence intensity decrease, being τ_p the phosphorescence lifetime of acetone molecules (Kaskan and Duncan 1950).
However, the source term can be eliminated by the following rescaling:

$$n_2(x,y,z,t) = N_0 \exp(-\frac{t}{\tau_p})p(x,y,z,t) \tag{39}$$

where N_0 is the total number of tagged molecules initially created and the new unknown probability density $p(x,y,z,t)$ obeys the equation:

$$\frac{\partial p}{\partial t} + u_x(y,z)\frac{\partial p}{\partial x} = \mathscr{D}_{12}\nabla^2 p. \tag{40}$$

Since the tagged molecules displacements are small when compared with the channel length L_x, the x-coordinate domain is considered unbounded. Accordingly, p is defined in the domain $\Omega = \{(x,y,z) \in \mathscr{R}_3 : -\infty < x < +\infty, -L_y/2 < y < L_y/2, -L_z/2 < z < L_z/2\}$. Under the assumption that collisions with channel walls do not cause tagged molecules absorption by promoting a non-radiative deexcitation, the following boundary conditions can be assigned at walls:

$$\frac{\partial p}{\partial z} = 0, z = \pm L_z/2 \qquad \frac{\partial p}{\partial y} = 0, y = \pm L_y/2. \tag{41}$$

The initial probability distribution is assigned as $p(x,y,z,0) = p_0(x,y,z)$. The shape of $p_0(x,y,z)$ is related to the way the gas is illuminated by the laser beam. In the following developments, it is assumed that a thin cylindrical beam produces a y-independent initial state of the form:

$$p_0(x,z) = \begin{cases} \frac{1}{V_0} & (x,y,z) \in \mathscr{C}_0 \\ 0 & (x,y,z) \notin \mathscr{C}_0 \end{cases} \tag{42}$$

where $\mathscr{C}_0$ is the set $\mathscr{C}_0 = \{(x,y,z) \in \mathscr{R}_3 : x^2 + z^2 < r_0^2, -L_y/2 < y < L_y/2\}$ and $V_0 = \pi r_0^2 L_y$ its volume.
The relationship between the velocity field u_x and the displacement $s_x(y,t)$ can be easily obtained from Eq. (40). Since the displacement is obtained as a function of y, it is useful to introduce the probability $P_{xz}(x,y,z,t)$ that a molecule has a position (x,z) on a plane at fixed y:

$$P_{xz}(x,y,z,t) = \frac{p(x,y,z,t)}{P_y(y,t)}, \quad P_y(y,t) = \int p(x,y,z,t)\,dx\,dz. \tag{43}$$

The displacement is now obtained as:

$$s_x(y,t) = \int x P_{xz}(x,y,z,t)\,dx\,dz = \frac{1}{P_y(y,t)}\int x p(x,y,z,t)\,dx\,dz. \tag{44}$$

It is shown that $P_y(y,t)$ is a constant because of the symmetry of the initial state. Integrating Eq. (40) over x and z while taking into account the boundary conditions (41) leads to the following for $P_y(y,t)$

$$\frac{\partial P_y}{\partial t} = \mathscr{D}_{12}\frac{\partial^2 P_y}{\partial y^2} \tag{45}$$

where $-\frac{L_y}{2} < y < \frac{L_y}{2}$ and $\frac{\partial P_y}{\partial y} = 0$ at $y = \pm\frac{L_y}{2}$. Since the illumination can be assumed to be uniform along the beam, as confirmed by experiments, the initial state does not depend on y. Hence $P_y(y,0) = P_0$, being P_0 a constant. As a matter of fact, it can be immediately seen that the function $P_y(y,t) = P_0$ is a solution of Eq. (45) and, because of the uniqueness theorem, it is the only solution with the prescribed initial state.

The evolution equation for $s_x(y,t)$ is readily obtained by multiplying Eq. (40) by x and integrating over x and z:

$$\frac{\partial s_x}{\partial t} = \overline{u}_x(y,t) + \mathscr{D}_{12}\frac{\partial^2 s_x}{\partial y^2}, \tag{46}$$

with initial state $s_x(y,0) = 0$ and boundary conditions $\frac{\partial s_x}{\partial y} = 0$ at $y = \pm\frac{L_y}{2}$. The velocity $\overline{u}_x(y,t)$ is defined as:

$$\overline{u}_x(y,t) = \frac{\int u_x(y,z)p(x,y,z,t)\,dxdz}{P_0}. \tag{47}$$

As is clear, tagged molecules displacement evolve under the action of the average velocity $\overline{u}_x(y,t)$, which is determined by the gas velocity field $u_x(y,z)$ and the spatial molecules distribution described by $p(x,y,z,t)$. If $u_x(y,z) \approx u_x(y)$, as it happens in the central part of the channel when $L_z \gg L_y$, then $\overline{u}_x(y,t) \approx u_x(y)$ as long as tagged particles positions remain confined in the region where $\partial u_x/\partial z \approx 0$. The above considerations impose a limit to the measurement duration which should not exceed a limit time t_l, after which the tagged molecules z coordinates variance would be larger than channel width. A rough estimation of t_l is given by the following expression:

$$t_l = \frac{L_z^2}{2\mathscr{D}_{12}}. \tag{48}$$

For $t < t_l$, the approximation $\overline{u}_x(y,t) \approx u_x(y)$ holds and Eq. (46) takes the form:

$$\frac{\partial s_x}{\partial t} = u_x(y) + \mathscr{D}_{12}\frac{\partial^2 s_x}{\partial y^2}. \tag{49}$$

The solution of Eq. (49), with initial state and boundary conditions stated above, can be given in closed form as (Crank 1975):

$$s_x(y,t) = (W_0,u_x)t\,W_0 + \sum_{k=1}^{\infty}\tau_k(W_k,u_x)(1-e^{-t/\tau_k})W_k(y). \tag{50}$$

In Eq. (50), the symbol $(\,,\,)$ denotes the scalar product of any two functions in $(-\frac{L_y}{2},+\frac{L_y}{2})$, defined as

$$(f,g) = \int_{-\frac{L_y}{2}}^{+\frac{L_y}{2}} f(y)g(y)\,dy. \tag{51}$$

The functions

$$W_k(y) = \begin{cases} \frac{1}{\sqrt{L_y}}, & k=0 \\ \sqrt{\frac{2}{L_y}}\cos\left(\frac{2\pi k}{L_y}y\right), & k=1,\ldots,\infty \end{cases} \tag{52}$$

obey the conditions $(W_k,W_l) = \delta_{kl}$, being δ_{kl} the Kronecker's delta. The time constants $\tau_k = \frac{1}{\mathscr{D}_{12}}\left(\frac{L_y}{2\pi k}\right)^2$ characterize the exponential time evolution of the amplitudes associated to the spatial modes W_k.
The direct linear relationship between the velocity field u_x and the average displacement s_x can be seen more clearly by recasting Eq. (50) in the form:

$$s_x(y,t) = \int_{-\frac{L_y}{2}}^{+\frac{L_y}{2}} G(y,y'|t)u_x(y')\,dy', \tag{53}$$

where the Green function $G(y,y'|t)$ takes the form:

$$G(y,y'|t) = W_0(y)W_0(y')t + \sum_{k=1}^{\infty}\tau_k(1-e^{-t/\tau_k})W_k(y)W_k(y') \tag{54}$$

References

1977; *Classical kinetic theory of fluids*. J. Wiley & Sons, New York

Arkilic E B, Breuer K S, Schmidt M A, 2001; Mass flow and tangential momentum accommodation in silicon micromachined channels. Journal of Fluid Mechanics 437:29–43

Bird G A, 1994; *Molecular Gas Dynamics and the Direct Simulation of Gas Flows*. Clarendon Press, Oxford

Bruno D, Catalfamo C, Laricchiuta A, Giordano D, Capitelli M, 2006; Convergence of Chapman-Enskog calculation of transport coefficients of magnetized Argon plasma. Phys Plasmas 13(7):072307

Cattafesta L N, Sheplak M, 2011; Actuators for active flow control. Annual Review of Fluid Mechanics 43:247–272

Cercignani C, 1988; *The Boltzmann Equation and Its Applications*. Springer-Verlag, Berlin

Colin S, 2005; Rarefaction and compressibility effects on steady and transient gas flows in microchannels. Microfluidics and Nanofluidics 1:268–279

Colin S, 2012; Gas microflows in the slip flow regime: a critical review on convective heat transfer. Journal of Heat Transfer-Transactions of the ASME 134:020908

Colin S, Lalonde P, Caen R, 2004; Validation of a second-order slip flow model in rectangular microchannels. Heat Transfer Engineering 25:23–30

Crank J, 1975; *The Mathematics of Diffusion*. Clarendon Press, s ed.

Dongari N, Sharma A, Durst F, 2009; Pressure-driven diffusive gas flows in micro-channels: from the knudsen to the continuum regimes. Microfluidics and Nanofluidics 6(5):679–692

ElBaz A, Pitz R, 2012; n_2o molecular tagging velocimetry. Applied Physics B: Lasers and Optics 106(4):961–969. doi:10.1007/s00340-012-4872-5

Elsnab J R, Maynes D, Klewicki J C, Ameel T A, 2010; Mean flow structure in high aspect ratio microchannel flows. Experimental Thermal and Fluid Science 34:1077–1088

Ewart T, Perrier P, Graur I, Meolans J G, 2006; Mass flow rate measurements in gas micro flows. Experiments in Fluids 41:487–498

Ferziger J H, Kaper H G, 1972; *Mathematical Theory of Transport Processes in Gases*. North-Holland

Gendrich C P, Koochesfahani M M, Nocera D G, 1997; Molecular tagging velocimetry and other novel applications of a new phosphorescent supramolecule. Experiments in Fluids 23:361–372

Hammer P, Pouya S, Naguib A, Koochesfahani M, 2013; A multi-time-delay approach for correction of the inherent error in single-component molecular tagging velocimetry. Measurement Science and Technology 24:105302

Hu H, Koochesfahani M M, 2006; Molecular tagging techniques for micro-flow and micro-scale heat transfer studies. In *Proceedings of FEDSM09*. ASME, FEDSM2009–78059

Ismailov M, Schock H, Fedewa A, 2006; Gaseous flow measurements in an internal combustion engine assembly using molecular tagging velocimetry. Experiments in Fluids 41:57–65

Kaskan W E, Duncan A B F, 1950; Mean lifetime of the fluorescence of acetone and biacetyl vapors. The Journal of Chemical Physics 18(4):427–431

Koochesfahani M M, 1999; Molecular tagging velocimetry (MTV): progress and applications. In *30th AIAA Fluid Dynamics Conference, Norfolk, VA*. AIAA99–3786

Koochesfahani M M, Nocera D G, 2007; Molecular tagging velocimetry. In C Tropea, A L Yarin, J F Foss, eds., *Handbook of Experimental Fluid Dynamics*, chap. 5.4. Springer, 362–382

Kovach K M, LaBarbera M A, Moyer M C, Cmolik B L, van Lunteren E, et al., 2015; In vitro evaluation and in vivo demonstration of a biomimetic, hemocompatible, microfluidic artificial lung. Lab Chip 15:1366–1375. doi:10.1039/C4LC01284D. URL `http://dx.doi.org/10.1039/C4LC01284D`

Lempert W R, Boehm M, Jiang N, Gimelshein S, Levin D, 2003; Comparison of molecular tagging velocimetry data and direct simulation Monte Carlo simulations in supersonic micro jet flows. Experiments in Fluids 34:403–411

Lempert W R, Ronney P, Magee K, Gee K R, Haugland R P, 1995; Flow tagging velocimetry in incompressible flow using photo-activated nonintrusive tracking of molecular motion (PHANTOMM). Experiments in Fluids 18:249–257

Louisos W, Hitt D L, 2005; Influence of wall heat transfer on supersonic MicroNozzle performance. Journal of Spacecraft and Rockets 49:1123–1131

Lu C J, Steinecker W H, Tian W C, Oborny M C, Nichols J M, et al., 2005; First-generation hybrid MEMS gas chromatograph. Lab on a Chip 5:1123–1131

Matsuda Y, Misaki R, Yamaguchi H, Niimi T, 2011a; Pressure-sensitive channel chip for visualization measurement of micro gas flows. Microfluidics and Nanofluidics 11:507–510

Matsuda Y, Uchida T, Suzuki S, Misaki R, Yamaguchi H, et al., 2011b; Pressure-sensitive molecular film for investigation of micro gas flows. Microfluidics and Nanofluidics 10:165–171

Maurer J, Tabeling P, Joseph P, Willaime H, 2003; Second-order slip laws in microchannels for helium and nitrogen. Physics of Fluids 15:2613–2621

Morini G L, Yang Y, Chalabi H, Lorenzini M, 2011; A critical review of the measurement techniques for the analysis of gas microflows through microchannels. Experimental Thermal and Fluid Science 35:849–865

Niu C, Hao Y z, Li D, Lu D, 2014; Second-order gas-permeability correlation of shale during slip flow. SPE Journal 19:786–792

Perrier P, Graur I A, Ewart T, Meolans J G, 2011; Mass flow rate measurements in microtubes: from hydrodynamic to near free molecular regime. Physics of Fluids 23:042004

Pitakarnnop J, Varoutis S, Valougeorgis D, Geoffroy S, Baldas L, et al., 2010; A novel experimental setup for gas microflows. Microfluidics and Nanofluidics 8:57–72

Pitz R W, Lahr M D, Douglas Z W, Wehrmeyer J A, Hu S, et al., 2005; Hydroxyl tagging velocimetry in a supersonic flow over a cavity. Applied Optics 44:6692–6700

Samouda F, Barrot C, Colin S, Baldas L, Laurien N, 2012a; Analysis of gaseous flows in microchannels by molecular tagging velocimetry. In *Proceedings of the ASME 2012 10th International Conference on Nanochannels, Microchannels and Minichannels (ICNMM2012)*. ASME. ISBN 978-0-7918-4479-3, 221–228

Samouda F, Brandner J J, Barrot C, Colin S, 2012b; Velocity field measurements in gas phase internal flows by molecular tagging velocimetry. Journal of Physics: Conference Series - Proceedings of 1st European Conference on Gas MicroFlows (GASMEMS2012) 362:012026

Samouda F, Colin S, Barrot C, Baldas L, Brandner J J, 2015; Micro molecular tagging velocimetry for analysis of gas flows in mini and micro systems. Microsystem Technologies 21:527–537

Schembri F, Bodiguel H, Colin A, 2015; *Velocimetry in microchannels using photobleached molecular tracers: a tool to discriminate solvent velocity in flows of suspensions*

Seungdo A, Gupta N K, Gianchandani Y B, 2014; A Si-micromachined 162-stage two-part Knudsen pump for on-chip vacuum. Journal of Microelectromechanical Systems 23:406–416

Sharipov F, 2011; Data on the velocity slip and temperature jump on a gas-solid interface. Journal of Physical and Chemical Reference Data 40:023101

Stier B, Koochesfahani M M, 1999; Molecular Tagging Velocimetry (MTV) measurements in gas phase flows. Experiments in Fluids 26:297–304

Sugii Y, Okamoto K, 2006; Velocity measurement of gas flow using micro piv technique in polymer electrolyte fuel cell. In *Proceedings of 4th International Conference on Nanochannels, Microchannels and Minichannels*. ASME, 533–538

Thompson B R, Maynes D, Webb B W, 2005; Characterization of the hydrodynamically developing flow in a microtube using MTV. Journal of Fluids Engineering 127:1003–1012

Yang Y, Gerken I, Brandner J J, Morini G L, 2014; Design and experimental investigation of a gas-to-gas counter flow micro heat exchanger. Experimental Heat Transfer 27:340–359

Yoon S Y, Ross J W, Mench M M, Sharp K V, 2006; Gas-phase particle image velocimetry (PIV) for application to the design of fuel cell reactant flow channels. Journal of Power Sources 160:1017–1025

Zhang W M, Meng G, Wei X, 2012; A review on slip models for gas microflows. Microfluidics and Nanofluidics 13:845–882